SUPPLEMENTARY: Material and Methods

Here we describe the detailed methods for calculating the energy budgets of both gray and white matter in the human brain as well as for the rat brain. Below we provide details of calculation for the cost of action potential conduction along neuronal axons and dendrites use of energy to transport ions for pyramidal cells and GABAergic interneurons, and energetic costs for synaptic transmission.

SI Text, Section A - Gray matter energy budget for human brain

Calculation of energy budget for gray matter (E_{gm}) has contributions from demands of excitatory (E_e) and inhibitory (E_i) neurons and individual glial cells (E_g),

$$E_{gm} = 0.8N_n^{gm}E_e + 0.2N_n^{gm}E_i + N_g^{gm}E_g \quad \text{(S1)}$$

where N_n^{gm} = 13.63 billion and N_g^{gm} = 19.15 billion, respectively, are the total number of neurons and glial cells in gray matter [1] (**Section D**), where 80% of all cortical neurons are excitatory (glutamatergic) pyramidal cells and 20% are inhibitory (GABAergic) interneurons [2], respectively. E_e, E_i, and E_g were calculated by,

$$\begin{aligned} E_e &= E_{HK}^e + E_{RP}^e + E_{AP}^e f_e + E_{ST}^e f_e + E_{glu}^e f_e + E_{Ca}^e f_e \\ E_i &= E_{HK}^i + E_{RP}^i + E_{AP}^i f_i + E_{ST}^i f_i + E_{GABA}^i f_i + E_{Ca}^i f_i \\ E_g &= E_{HK}^g + E_{RP}^g + E_{Ca}^g f_e \end{aligned} \quad \text{(S2a-c)}$$

where superscripted x in E_Y^x represents 'e' or 'i' or 'g' for individual excitatory or inhibitory neurons or glial cells and subscripted *Y* in E_Y^x represents the different cellular functions like energy costs for housekeeping ($E_{HK}^e, E_{HK}^i, E_{HK}^g$), maintenance of membrane resting potentials ($E_{RP}^e, E_{RP}^i, E_{RP}^g$), action potential conduction (E_{AP}^e, E_{AP}^i), synaptic transmission (E_{ST}^e, E_{ST}^i), glutamate or GABA recycling (E_{glu}^e, E_{GABA}^i), and presynaptic calcium entry into neurons (E_{Ca}^e, E_{Ca}^i). The terms f_e and f_i in **eqs. S2a-c** represent the firing rates of excitatory and inhibitory neurons respectively, where we assume that inhibitory neurons have approximately twice the firing rate of excitatory neurons as observed on

average [3], and the glial calcium term in **eq. S2c** (E_{Ca}^{g}) is directly related to firing rate of excitatory neurons, where it was reported that glial cells have significant active calcium responses accompanying spiking activity of neurons [4, 5]. Neuronal activity-dependent transmitter release raises calcium influx in astrocytes by activating metabotropic glutamate receptors. These calcium transients in astrocytes [4, 6, 7] are recorded in about half of the neuronal calcium response and are observed to be associated with a transient arterial vasodilation [5, 8]. Hence, energy demand for glial cells in the cerebrum (E_g) includes energy costs for active calcium signaling responses. For a rough estimation of E_{Ca}^{g}, based on experiments [4, 6, 7], we calculated that

$$E_{Ca}^{g} = \gamma E_{Ca}^{n} \qquad \text{(S2d)}$$

where E_{Ca}^{n} represents the excitatory (E_{Ca}^{e}) neuronal calcium activities (see above), and γ can range from 0 to 1, but we assumed an optimized value of 0.8 is used to fit the PET imaging data best in this paper) based on the observation that transients of glial calcium [4, 6, 7] and neuronal calcium [5, 8] are comparable.

By combining **eq. S2** into **eq. S1** we derived E_{gm} in terms of different cellular functions like housekeeping (E_{HK}^{gm}), resting potential (E_{RP}^{gm}), action potential (E_{AP}^{gm}), synaptic transmission (E_{ST}^{gm}), neurotransmitter cycling (E_{cyc}^{gm}, represents both excitatory E_{glu}^{gm} and inhibitory E_{GABA}^{gm}), and presynaptic calcium entry into neurons (E_{Ca}^{gm}),

$$
\begin{aligned}
E^{gm}_{HK} &= 0.8N^{gm}_{n}E^{e}_{HK} + 0.2N^{gm}_{n}E^{i}_{HK} + N^{gm}_{g}E^{g}_{HK} \\
E^{gm}_{RP} &= 0.8N^{gm}_{n}E^{e}_{RP} + 0.2N^{gm}_{n}E^{i}_{RP} + N^{gm}_{g}E^{g}_{RP} \\
f_e E^{gm}_{AP} &= 0.8N^{gm}_{n}E^{e}_{AP}f_e + 0.2N^{gm}_{n}E^{i}_{AP}f_i \\
f_e E^{gm}_{ST} &= 0.8N^{gm}_{n}E^{e}_{ST}f_e + 0.2N^{gm}_{n}E^{i}_{ST}f_i \\
f_e E^{gm}_{cyc} &= 0.8N^{gm}_{n}E^{e}_{glu}f_e + 0.2N^{gm}_{n}E^{i}_{GABA}f_i \\
f_e E^{gm}_{Ca} &= 0.8N^{gm}_{n}E^{e}_{Ca}f_e + 0.2N^{gm}_{n}E^{i}_{Ca}f_i + N^{gm}_{g}E^{g}_{Ca}f_e \\
E_{gm} &= E^{gm}_{HK} + E^{gm}_{RP} + f_e(E^{gm}_{AP} + E^{gm}_{ST} + E^{gm}_{cyc} + E^{gm}_{Ca})
\end{aligned}
\qquad \text{(S3a-g)}
$$

and where **eq. S3g** can be further broken into signaling ($E^{gm}_{signaling}$) and nonsignaling ($E^{gm}_{nonsignaling}$) components with the assumption that $f_i \approx 2f_e$ (see above),

$$
\begin{aligned}
E_{gm} &= E^{gm}_{nonsignaling} + E^{gm}_{signaling} \\
E^{gm}_{nonsignaling} &= E^{gm}_{HK} + E^{gm}_{RP} \\
&= 0.8N^{gm}_{n}(E^{e}_{HK} + E^{e}_{RP}) + 0.2N^{gm}_{n}(E^{i}_{HK} + E^{i}_{RP}) + N^{gm}_{g}(E^{g}_{HK} + E^{g}_{RP}) \\
E^{gm}_{signaling} &= f_e(E^{gm}_{AP} + E^{gm}_{ST} + E^{gm}_{glu} + E^{gm}_{Ca}) \\
E^{e}_{nonsignaling} &= E^{e}_{HK} + E^{e}_{RP} \\
E^{i}_{nonsignaling} &= E^{i}_{HK} + E^{i}_{RP} \\
E^{g}_{nonsignaling} &= E^{g}_{HK} + E^{g}_{RP} \\
E^{e}_{signaling} &= f_e(E^{e}_{AP} + E^{e}_{ST} + E^{e}_{glu} + E^{e}_{Ca}) \\
E^{i}_{signaling} &= f_i(E^{i}_{AP} + E^{i}_{ST} + E^{i}_{gaba} + E^{i}_{Ca}) \\
E^{g}_{signaling} &= f_e E^{g}_{Ca}
\end{aligned}
\qquad \text{(S4a-i)}
$$

Note that $E^{gm}_{nonsignaling}$ is solely dependent on number of cells (i.e., mass of brain tissue), whereas $E^{gm}_{signaling}$ relies on both brain tissue mass and neuronal firing rate. In addition, for individual cells, the energy cost can also divided into nonsignaling- and signaling-dependent, i.e., cell nonsignaling costs mainly include housekeeping and resting potential (S4d-f), while cell signaling costs mainly include costs associated with action potential, synaptic transmission, glutamate or GABA transmitter recycling, and calcium activities. Glial cell signaling cost mainly support for calcium activity. Below we describe the calculation of each of the different cellular components ($E^{gm}_{HK}, E^{gm}_{RP}, E^{gm}_{AP}, E^{gm}_{ST}, E^{gm}_{cyc}, E^{gm}_{Ca}$) in detail.

SI Text, Section A.1 - Cellular housekeeping (E_{HK}^{gm}) for individual neuronal and glial cells

A long-term unsolved issue in calculating brain energy budget is the amount of energy used for pure nonsignaling molecular activities of a neuronal or a glial cell. The energy demand for nonsignaling molecular processes of a brain cell could be viewed, and as we have assumed, as the necessary energy to support a body cell of the same mass to survive under normal conditions. This amount of energy demand should therefore be independent of external stimuli and/or any internal signaling processes, but mainly depend on the cellular mass for supporting all types of function associated with biosynthesis, e.g., protein and lipid synthesis, cytoskeletal rearrangements, etc. Thus we term this amount of energy as housekeeping energy, E_{HK}^{gm}. The whole body basal metabolic rate for human in the resting state demands $E_{body} \sim 60$ watts [9, 10] for a given body mass (M_{body}) of 65 kg. Considering a cerebrum mass ($M_{cerebrum}$) of 1.233 kg, given by the sum of white (M_{wm}) and gray (M_{gm}) matter (**Section E**), the basal energy to support the cerebrum nonsignaling cellular housekeeping processes can be calculated as

$$E_{HK}^{gm} = (M_{brain} / M_{body}) \times E_{body} = (1.233/65) \times 60 = 1.14 \text{ watts} \qquad \text{(S5a)}$$

where 1 watt is equivalent to 1.9707×10^{19} ATP/s[11] or 32.72 μmol of ATP/s given that the Avogadro constant is 6.023×10^{23}/mol. Given that one of mole glucose can generate 33.6 mole of ATP with oxygen-to-glucose index (OGI) of 5.3 on average [12, 13], 32.72 μmol of ATP/s is equivalent to glucose units of 0.974 μmol/s or 58.43 μmol/min. For a given cerebrum of 1.233 kg weight, glucose units of 58.43 μmol/min converts to 0.0474 μmol/min/g. Thus E_{HK}^{gm} of 1.14 watts corresponds to 0.054 μmol of glucose/min/g. A conversion factor between ATP/s and μmol/min for glucose is k, which is 2.965×10^{-18}.

Based on recent experimental reports [1], we calculated the mass of individual glial cells m_g = 12.3 ng and neurons m_n = 29.5 ng (**Section F**). Given the fact that the human cerebrum contains

total number of neurons N_n = 16.34 billion and number of glial cells N_g = 60.84 billion (**Section D**), and if we simply assume that resting metabolic cost of a cell is proportional to its mass, i.e., $E^n_{HK} / E^g_{HK} = m_n / m_g$, then the total cerebrum housekeeping energy E_{HK} is given by

$$E^{gm}_{HK} = N_n E^n_{HK} + N_g E^g_{HK} \quad \text{(S5b)}$$

or to consider excitatory and inhibitory neuron to be more precise,

$$E^{gm}_{HK} = 0.8 N_n E^e_{HK} + 0.2 N_n E^i_{HK} + N_g E^g_{HK}. \quad \text{(S5c)}$$

Solving **eq. S5** we get $E^n_{HK} = 3.23 \times 10^8$ ATP/sec (or $E^e_{HK} = 3.46 \times 10^8$ ATP/sec and $E^i_{HK} = 2.3 \times 10^8$ ATP/sec (histological measurements in rodent brain [14] suggest that axon and dendrite lengths of inhibitory neurons are about half of those of pyramidal cells. The cell body of inhibitory cells is viewed as a ball with diameter round 15 μm while pyramidal cell body is viewed as a cone with diameter and length about 25 μm, thus the total volume/mass of inhibitory cell is about 2/3 of a pyramidal cell) and $E^g_{HK} = 1.37 \times 10^8$ ATP/sec. Since we used a different method in calculating housekeeping costs, the terms E^n_{HK} and E^g_{HK} here should, by definition, include the energy supporting all the necessary molecular activities like synthesis of proteins, lipids, cholesterols, etc. (i.e., biosynthesis).

SI Text, Section A.2 - Maintaining resting potential (E^{gm}_{RP}) for neuronal and glial cells

The energy required to maintain the resting potential of a neuronal or glial cell due to the leakiness of the cell membrane to ions, and is calculated as follows

$$E_{RP} = (V_{Na} - V_{RP})(V_{RP} - V_K) \,/\, [F R_m (V_{RP} + V_{Na} - 3V_K)] \quad \text{(S6)}$$

where E_{RP} has the unit of ATP/sec, V_{Na}, V_K and V_{RP} represent the Nernst potentials for Na^+, K^+ and resting membrane potential, respectively. Note that we used V_{Na} = 50 mV and V_K = -100 mV for all types of cells, V_{RP} = -70 mV for both pyramidal glutamatergic neurons and GABAergic interneurons, while V_{RP} = -80 mV for glial cells; F is the Faraday constant (96485.3365 sA/mol), and

R_m is the input resistance of cell membrane (100 MΩ for pyramidal cells [15-17], 200 MΩ for interneurons [16-18], and 200 MΩ for glial cells [16, 17, 19] in gray matter) respectively. Calculations show that E_{RP}^{gm} is given by the sum of the excitatory (E_{RP}^{e}), inhibitory (E_{RP}^{i}), and glial (E_{RP}^{g}) components; i.e., $E_{RP}^{e} = 6.8 \times 10^8$ ATP/sec, $E_{RP}^{i} = 3.4 \times 10^8$ ATP/sec, and $E_{RP}^{g} = 2.54 \times 10^8$ ATP/sec respectively.

SI Text, Section A.3 - Cost of action potential conduction (E_{AP}^{gm}) for individual neurons

Action potential conduction along neuronal axons and dendrites use energy to pump out intracellular Na^+ (i.e., 1 ATP energy corresponding to 3 Na^+) entering during action potential process. Hence the energy for action potential E_{AP} in individual neurons is calculated by

$$E_{AP} = f \Delta Q_{Na} / 3 \qquad \text{(S7)}$$

where f is the averaged firing rate of a neuron, and ΔQ_{Na} is the total Na^+ charge during action potential process. As the methods used in recent reports, the minimum amount of Na^+ influx is needed to charge the membrane to depolarize to the peak of an action potential is $\Delta Q_{min} = S\, C_m\, \Delta V$, where S is the membrane surface area, C_m is the membrane capacitance, and ΔV is the amplitude of action potential measured from the spike threshold to the peak of the action potential. The actual Na^+ charge is always larger than the minimum Na^+ influx manly because Na^+ influx and K^+ efflux has an overlap in reality, thus $\Delta Q_{Na} = \varepsilon \Delta Q_{min} = \varepsilon S\, C_m\, \Delta V$, where ε is the Na^+ influx to K^+ efflux overlap ratio. Experimental studies indicated that warm-blooded animals have a much smaller ε (≈ 1.3-1.6 for cortical axons in pyramidal cells and 2-2.5 for interneurons) than cold-blooded animal (4-15 for squid axon in cold temperature) [20-23], and ionic channel kinetics and warm body temperature may act as critical factors in facilitating energy efficiency in reducing the dynamic overlap level of Na^+ influx and K^+ efflux [20-24]. The membrane surface area S of a neuron was calculated as

$$S = S_{axon} + S_{dend} + S_{soma} \qquad \text{(S8)}$$

where axon area $S_{axon} = \pi$ d L with axon diameter d = 0.3 mm (same as rat brain) and axon length L_{axon}. The calculation of human neuron size is as follows.

It was recently demonstrated [25] that individual neuronal mass m of mammalian and human brains follows the same scaling function with neuronal density ρ, i.e., $m = 0.649\ \rho^{-1.004}$. Experimental data gives neuronal density $\rho = N_{gm}/M_{gm} = 2.14 \times 10^7$ neurons/g, with $N_{gm} = 13.63 \times 10^9$ neurons and $M_{gm} = 638.37$ g for mass for human brain gray matter, and $\rho = 31.02 \times 10^6 / 0.77 = 4.03 \times 10^7$ neurons/g for rat brain gray matter. So the weight ratio between human gray matter neuron and rat neuron is $0.649 \times (2.56\times10^7)^{-1.004} / (0.649 \times (4.03\times10^7)^{-1.004} \approx 1.89$, which could also be used as the neuronal volume ratio given the brain tissue density is 1.05 g/mL. We simply assumed that neurons of different species have dendrites and axons of same diameter, but with different lengths. The measured total axon length of a typical rat pyramidal cell is about 4 cm and dendrite length of 0.44 cm [14], whereas the total axon length of a human brain pyramidal neuron should then be 7.56 cm based on a recently established relation of cross-species neuroanatomical data [1, 25]. The typical length of dendrites in the pyramidal cells is about $L_{axon}/9$. For action potentials conducted in dendrite, their averaged amplitude of action potential is computed as 50 mV because of passive propagation decay, that is about half of the axonal action potential [16]. The pyramidal cell somatic diameter D = 25 μm and height 25 μm gives the somatic area $S_{soma} = \pi (D/2)^2 + \pi D^2/2$.

For GABAergic interneurons, their size is usually smaller than pyramidal cells, and histological measurements suggest that axon and dendrite lengths are about half of those of pyramidal cells and cell body diameter is about 15 μm [14]. Based on the above parameters and recent morphological measurements, we compute that total action potential energy costs (E_{AP}^{gm}) has excitatory (E_{AP}^{e}) and inhibitory (E_{AP}^{i}) neuronal components

$$E_{AP}^{e} = f_e\ \Delta Q_{Na}^{e} / 3$$
$$E_{AP}^{i} = f_i\ \Delta Q_{Na}^{i} / 3 \qquad \text{(S9a-b)}$$

and the results show E^{e}_{AP} = 2.65 × 10^8 ATP/sec and E^{i}_{AP} = 3.09 × 10^8 ATP/sec for neurons at 1 Hz firing rate with $e$values of 1.5 and 2.2 for excitatory and inhibitory processes, respectively.

SI Text, Section A.4 - Cost of synaptic transmission (E^{gm}_{ST})

We used the same methods described by previous reports for calculating presynaptic and postsynaptic cost for neurons (i.e., ion influx through ionotropic receptors) in either gray matter [16] or white matter [26], as shown by,

$$E_{ST} = f\, r_{ves}\, n_{bouton}\, E_{ves} \qquad \text{(S10)}$$

where f is the average firing rate of a neuron, r_{ves} is the vesicle neurotransmitter release probability and its value is believed to decrease exponentially with increasing value of f (e.g., 0.7 for ~0.1 Hz firing rate, 0.64 for ~1 Hz firing rate, 0.45 for ~4 Hz firing rate at temperature of 37 °C [16, 27]. The release probability vs. glutamatergic firing rate can be described by the fitting equation, r_{ves} = 0.6 exp(-f/10.6)+0.128), where f is 1 Hz, n_{bouton} is the number of boutons in presynapntic terminals (i.e., 8000 boutons for rat pyramidal cells and n_{bouton} = 15,100 (i.e., 8000 × 1.89) for human pyramidal cells, where 1.89 is the size ratio between human gray matter neuron and rat neuron; see **Section A.3**), and E_{ves} is the energy cost for releasing one vesicle of glutamate. We assumed E_{ves} to be 1.64 × 10^5 ATP molecules, which is the same as previous study[16]. For details of the molecular processes involved in exocytosis and endocytosis of vesicles, we refer the original references for gray matter [16] and white matter [26].

The GABAergic synaptic transmission costs energy captured by **eq. S10** but with relatively high firing rate (i.e., f for interneurons is taken conservatively as 2 times higher than that of pyramidal cells although 4 times was reported [28]) with half number of synaptic boutons because of shorter dendrite length in interneurons than in pyramidal cells. In addition, the GABA release probability vs. GABAergic firing rate can be described by the equation as r_{ves} = exp(-f/10.6), where f is 2 Hz. Based on the above parameters, we get the total energy costs for synaptic transmission

(E_{ST}^{gm}) with excitatory (E_{ST}^{e}) and inhibitory (E_{ST}^{i}) contributions, i.e., $E_{ST}^{e} = 1.58 \times 10^{9}$ ATP/sec ($1\times0.64\times15100\times1.64\times10^{5}$) for 1 Hz firing rate, and $E_{ST}^{i} = 2.05 \times 10^{9}$ ATP/sec ($2\times0.83\times7549\times1.64\times10^{5}$) for 2 Hz firing rate of GABA neurons. It should be noted, however, that the vesicle neurotransmitter release probability term in **eq. S10** needs better experimental validation.

SI Text, Section A.5 - Cost of neurotransmitter recycling (E_{glu}^{e} and E_{GABA}^{i})

Previous reports [16] have shown that 2.67 ATP molecules are required to recycle each glutamate molecule, with processes including H^{+} ion co-transport during glutamate pumping into vesicles (0.33 ATP), Na^{+} ion co-transport during astrocytic glutamate uptake (1.33 ATP), and glutamine synthesis from glutamate in astrocytes (1 ATP). With a total of 4,000 glutamate molecules in a vesicle, the cost of neurotransmitter cycling ($E_{recycling}$) is 10680 ATP (i.e., 2.67×4000). While glutamine uptake into neurons had been assumed to be passive [16], recent studies show that glutamine uptake into neurons is an active process [29-31] . Assuming ~1 ATP molecule for each glutamine molecule reuptake into glutamatergic neurons, the revised stoichiometry is 3.67 ATP molecules to recycle each glutamate molecule. This increases $E_{recycling}$ to 14,680 ATP molecules (i.e., 3.67×4000). Thus for each glutamatergic neuron the total cost for glutamate recycling in pyramidal cells is given by,

$$E_{glu}^{e} = f\, r_{ves}\, n_{bouton}\, E_{recycling} \qquad \text{(S11a)}$$

where f is the firing rate, r_{ves} is the vesicle neurotransmitter release probability, and n_{bouton} is the number of presynapntic terminals (see **Section A.4**). Similarly for each GABAergic neuron the total cost for GABA recycling in interneurons can be described as,

$$E_{GABA}^{i} = f\, r_{ves}\, n_{bouton}\, E_{recycling}\,. \qquad \text{(S11b)}$$

However previous reports [16] did not account for GABA recycling for inhibitory interneurons. The cost of GABA recycling may be higher than glutamate recycling [29-31]. Assuming the same glutamate recycling and GABA recycling costs and vesicle/bouton relations, we get $E_{glu}^{e} = 1.41 \times 10^{8}$ ATP/sec

(i.e., 1×0.64×15100×14680) for 1 Hz firing glutamatergic neurons, and $E^{i}_{GABA} = 1.82 \times 10^{8}$ ATP/sec (i.e., 2×0.82×7549×14680) for 2 Hz firing rate of GABAergic neurons.

SI Text, Section A.6 - Cost of calcium entry (E^{gm}_{Ca})

The presynaptic action potential triggers calcium influx ($e_{Ca} = 1.2 \times 10^{4}$ calcium per vesicle) in presynaptic terminals of individual neurons. It costs 1.2×10^{4} ATPs for the membrane to extrude those calcium for each vesicle (i.e., 1 ATP molecule corresponding to 1 Ca^{2+} ion) [16]. Hence, the total cost for calcium for individual neurons is

$$E_{Ca} = f \, r_{ves} \, n_{bouton} \, e_{Ca} \qquad \text{(S12)}$$

In equation **eq. S12** we used the same r_{ves} and n_{bouton} values described above (see **Section A.4**). It was reported that glial cells like astrocytes also have significant active calcium responses accompanying spiking activation of neurons. Neuronal activity-dependent transmitter release raises calcium influx in astrocytes by activating metabotropic glutamate receptors. These calcium transients in astrocytes are recorded in over half of the neuronal calcium response and are observed to be associated with a transient arterial vasodilation [5, 8]. Hence, for glial cells in the cerebrum, their energy costs need to include at least an active calcium signaling responses as shown by **eq. S2d**, where g can range from 0 to 1 (0.8 is used in this paper) and 'n' in E^{n}_{Ca} represents either excitatory (E^{e}_{Ca}) or inhibitory (E^{i}_{Ca}) neuron. Based on the above parameters, we get $E^{e}_{Ca} = 1.16 \times 10^{8}$ ATP/sec, $E^{i}_{Ca} = 2.83 \times 10^{7}$ ATP/sec, and $E^{g}_{Ca} = 9.24 \times 10^{7}$ ATP/sec for 1 Hz firing rate.

SI Text, Section B - White matter energy budget for human brain

Calculations of energy budget of white matter in the human brain (E_{wm}) is calculated by

$$\begin{aligned}
E_{wm} &= N^{wm}_{n} E_{g} + 0.8 N^{wm}_{n} E_{e} + 0.2 N^{wm}_{n} E_{i} + N_{axon} E_{axon} \\
E_{g} &= E^{g}_{HK} + E^{g}_{RP} + E^{g}_{Ca} f_{e} \\
E_{e} &= E^{e}_{HK} + E^{e}_{RP} + E^{e}_{AP} f_{e} + E^{e}_{ST} f_{e} + E^{e}_{glu} f_{e} + E^{e}_{Ca} f_{e} \\
E_{i} &= E^{i}_{HK} + E^{i}_{RP} + E^{i}_{AP} f_{i} + E^{i}_{ST} f_{i} + E^{i}_{GABA} f_{i} + E^{i}_{Ca} f_{i}
\end{aligned} \qquad \text{(S13a-d)}$$

where E_g, E_e and E_i are energy costs of individual glial cells, excitatory neurons, and inhibitory neurons in white matter, the total number of glial cells in white matter (N_g^{wm}) is 41.7 billion, the total number of neurons with unmyelinated axons in white matter (N_n^{wm}) is 2.7 billion [1] (**Section D**), and N_{axon} and E_{axon} are number and energy associated with myelinated axons in white matter (see below for details). It should noted that because of limited experimental data on neurons within white matter, the neuronal energy budgets for white matter assumed similar components (i.e., $E_{HK}^{gm}, E_{RP}^{gm}, E_{AP}^{gm}, E_{ST}^{gm}, E_{cyc}^{gm}, E_{Ca}^{gm}$) for individual cells as in gray matter (i.e., juxtapose **eqs. S3** and **S13**). However glial cells in white matter are diverse and based on some recent information on them, the following will be considered.

White matter in matured human or mammals is mainly composed of nerves that include, for example, an adult rat optic nerve may contain 100,000 myelinated axons [32] (where axons are projected from gray matter neurons) and at least three types of glial cells are involved for myelination and energy support , i.e., 15,650 astrocytes, 45,400 oligodendrocyte precursor cells (OPCs) and 381,000 oligodendrocytes [26, 33]. In other words, per 100,000 myelinated axons there are 442,050 other non-neural cells (= 15,650 + 45,400 + 381,000). We assume the ratio of different types of glial cell number in the human white matter is same as that found in the optic nerve, i.e., 1:2.9:24.345 for astrocytes : OPCs : oligodendrocytes. Considering the total glial cell number in white matter (N_g^{wm}; see **Section F**) is 41.7 billion, we calculated the total cell number for each type of glial cells, i.e., 1.476 billion astrocytes, 4.28 billion OPCs, 35.9 billion oligodendrocytes and 9.43 billion myelinated axons in white matter (= 41.7×(100,000/442,050) billion). The energy calculation for individual glial cells (E_{glial}) is then taken as

$$E_{glial} = E_{HK}^{glial} + E_{RP}^{glial} + E_{Ca}^{glial}(f) \quad \text{(S14)}$$

in white matter for astrocytes (R_m = 560 MΩ, V_{RP} = -80 mV, V_K = -100 mV, and V_{Na} = 50 mV), OPCs (R_m = 800 MΩ, V_{RP} = -80 mV, V_K = -100 mV, and V_{Na} = 50 mV) and oligodendrocytes (R_m = 200 MΩ, V_{RP} = -70 mV, V_K = -100 mV, and V_{Na} = 50 mV) [26]. We applied **eq. S6** to compute their resting potential energy as $E_{RP}^{astrocyte} = 9.05 \times 10^7$ ATP/sec, $E_{RP}^{oligodendrocyte} = 3.4 \times 10^8$ ATP/sec, and $E_{RP}^{OPC} = 8.51 \times 10^7$ ATP/sec, respectively. The housekeeping energy for each type of glial cell in white mater is simply taken as their sum, i.e., $E_{HK}^{glial} = 2.23 \times 10^8$ ATP/sec, though there should be some variance based on the mass differences of each type of cells.

As reported [6, 34] that astrocytes, OPCs and oligodendrocytes in white matter have active calcium responses related to spiking process through at least two different mechanisms, i.e., i) transmembrane calcium influx via voltage-operated calcium channels, and ii) calcium release from IP3-sensitive internal calcium stores. Hence, it is necessary to calculate energy cost for those calcium responses of glia in white matter, $E_{Ca}^{glial}(f)$ where *f* is the firing rate of neurons, and their calcium cost for individual cells is taken as 80% (same as in gray matter) of individual neuronal calcium responses [4, 6, 7]. In addition, we temporarily ignored other potential glial activities though recent experiments indicate that OPCs might have more diverse signaling responses like action potentials [35].

For each myelinated axon in white matter, the total 10.4 mm length (which is about 1.89 times longer than that of rodent axons) was occupied by 43 internodes of mean length of 240 μm and nodes of length 0.8 μm and diameter 0.77 μm[26]. We used the following equation to calculate the energy cost for nerves in white matter (see **eq. S13**)

$$N_{axon}E_{axon} = N_{axon}(E_{RP}^{axon} + E_{AP}^{axon} + E_{AP}^{node}) + N_{OPC}E_{ST}^{OPC} \quad \text{(S15)}$$

where the number of myelinated axons in white matter (N_{axon}) is 9.43 billion (see above), and cost of resting potential for each myelinated axon (E_{RP}^{axon}) is 1.24×10^8 ATP/sec as computed from **eq. S6** (see **Section A.3**) by the parameters of R_m of 0.55 billion Ω, and V_{RP} of -70 mV. The cost of action potential conducted along myelinated axon (E_{AP}^{axon}) is 5.87×10^7 ATP/sec as computed from **eq. S7**

(see **Section A.3**) by the parameters of myelinated axon length equal to 7.56 cm, diameter equal to 0.95 μm[26], capacitance equal to 0.08 μF/cm^2 and voltage amplitude of 100 mV, respectively. The cost of action potential initiated in node of Ranvier (E_{AP}^{node}) is 1.9 × 10^6 ATP/sec as computed from **eq. S7** (see **Section A.3**) by the parameters of node length equal to 0.8 μm, diameter 0.77 μm, capacitance equal to 1 μF/cm^2 and voltage amplitude of 100 mV, respectively. The interval of node is 240 μm resulting in 350 nodes for each myelinated axon.

In addition, as indicated in recent reports, there is no clear evidence for axo-axonal synapses in the myelinated axons, while there are synapse transmission processes between axons and OPCs [26, 36]. As indicated in recent report, when all presynaptic axons are stimulated, the post-synaptic current in an OPC could generate an average charge transfer of 366 fC. With 1 C including 6.24 × 10^{18} electrons, thus the cost for postsynaptic processes of an OPC will cost (E_{post}^{OPC}) 366 x 10^{15} x 6.24 × 10^{18}/3 = 7.61 x 10^5 ATP/s for 1 Hz neuronal firing rate. In addition, each OPC receives inputs from 141 axons and each of which releases 0.34 vesicles per action potential. Since each vesicle release may cost 23,400 ATP (consumed per vesicle released on presynaptic calcium flux, vesicle cycling, and neurotransmitter recycling)[26] the total energy needed for presynaptic processes in an OPC (E_{pre}^{OPC}) is calculated as 141 x 0.34 x 23400 = 1.12 x 10^6 ATP/s. So the synaptic transmission of an OPC (E_{ST}^{OPC}) will be $E_{pre}^{OPC} + E_{post}^{OPC}$ = 1.88 × 10^6 ATP/sec. Given that the number of OPCs (N_{OPC}) is 4.28 billion (see above), the total synaptic transmission of OPC is $N_{opc}E_{ST}^{OPC}$ = 8.05 × 10^{15} ATP/sec.

Based on the above calculations, metabolic cost of each type of cellular component in white matter can be further divided into two parts, i.e., signaling ($E_{signaling}^{wm}$) and nonsignaling ($E_{nonsignaling}^{wm}$),

$$
\begin{aligned}
&E_{wm} = E^{wm}_{nonsignaling} + E^{wm}_{signaling} \\
&E^{wm}_{nonsignaling} = E^{wm}_{HK} + E^{wm}_{RP} \\
&E^{wm}_{HK} = E^{astrocyte}_{HK} + E^{OPC}_{HK} + E^{oligodendrocyte}_{HK} + E^{e}_{HK} + E^{i}_{HK} \\
&E^{wm}_{RP} = E^{astrocyte}_{RP} + E^{OPC}_{RP} + E^{oligodendrocyte}_{RP} + E^{e}_{RP} + E^{i}_{RP} + E^{axon}_{RP} \\
&E^{wm}_{signaling} = f_e(E^{wm}_{AP} + E^{wm}_{ST} + E^{wm}_{glu} + E^{wm}_{Ca}) \qquad \text{(S16a-i)} \\
&E^{wm}_{AP} = E^{e}_{AP} + E^{i}_{AP} + E^{myelin}_{AP} + E^{node}_{AP} \\
&E^{wm}_{ST} = E^{e}_{ST} + E^{i}_{ST} + E^{axon}_{ST} \\
&E^{wm}_{glu} = E^{e}_{glu} + E^{i}_{GABA} \\
&E^{wm}_{Ca} = E^{e}_{Ca} + E^{i}_{Ca} + E^{astrocyte}_{Ca} + E^{oligodendrocyte}_{Ca}
\end{aligned}
$$

by which the whole energy cost of white matter based on **eq. S13** could be revised into a summation of nonsignaling ($E^{wm}_{nonsignaling}$) and signaling ($E^{wm}_{signaling}$) dependent items in **eq. S16a**. Note that $E^{wm}_{nonsignaling}$ described in **eq. S16b** includes costs for housekeeping (E^{wm}_{HK}) described in **Eq.16c** and maintenance of resting potentials (E^{wm}_{RP}) described in **eq. S16d**. Note that $E^{wm}_{signaling}$ described in **eq. S16e** includes costs for action potentials (E^{wm}_{AP}; **eq. S16f**), synaptic transmissions (E^{wm}_{ST}; **eq. S16g**), glutamate recycling (E^{wm}_{glu}; **eq. S16h**) and calcium activities (E^{wm}_{Ca}; **eq. S16i**). Terms like these were estimated similarly as in **Section A** for gray matter.

SI Text, Section C - Energy budget for rat brain

The calculation of rat gray matter energy budget also uses **eqs. S1-S16**, similar to human gray matter budget calculation, except the following parameters are different. Although rat brain is much smaller than the human brain, with gray matter mass of only 0.77 g [37], it contains 31.02 million neurons and 45.7 million glial cells in the gray matter, resulting in a ×2 higher neuronal density (40.3 million/g) and a ×1.98 higher glial cell density (59.4 million/g) than those of human gray matter (i.e., neuronal density 20.4 million/g and glial density 30.0 million/g). This results in a smaller rat neuronal size (i.e., unmyelinated axon is taken as 4 cm in length, 0.3 ηm in diameter, the total dendrite length is 4/9 cm with 0.9 ηm in diameter) and smaller glial cell size than human neuronal size (i.e., 1:1.89) and glial size (i.e., 1:1.89). In addition, the neuronal firing rate of rats in resting state

is around 3-5 Hz [16, 38], whereas human neuronal firing rate is around 0.5-1.5 Hz [28, 39-41]. These results will affect neuronal surface area and cellular mass in accounting for the signaling metabolism and housekeeping cost. Experimental observations [38, 39] have not reported significant differences in the electrophysiological properties (which include input resistance, resting potentials, and action potential amplitude) of both neuronal and glial cells in rat and human brain, except the cell size. Thus rat neurons and glia use same biophysical properties as those of human neurons, while lengths of dendrites and axons are 1/1.89 shorter.

SI Text, Section D - Number of neuronal and glial cells in gray and white matter

From recently reported number of neuronal (N_n = 16.34 billion) and glial (N_g = 60.84 billion) cells in the human cerebrum[1], we calculated number of neuronal and glial cells in white matter (N_n^{wm}, N_g^{wm}) and gray matter (N_n^{gm}, N_g^{gm}) by the following logic

$$N_n = N_n^{wm} + N_n^{gm} = N_n^{left\_wm} + N_n^{right\_wm} + N_n^{left\_gm} + N_n^{right\_gm} \quad \text{(S17a)}$$

$$N_g = N_g^{wm} + N_g^{gm} = N_g^{left\_wm} + N_g^{right\_wm} + N_g^{left\_gm} + N_g^{right\_gm} \quad \text{(S17b)}$$

In the right hemisphere of the human brain, the number of neurons in white matter ($N_n^{right\_wm}$) is 1.29 billion, number of neurons in gray matter ($N_n^{right\_gm}$) is 6.18 billion, number of glial cells in white matter ($N_g^{right\_wm}$) is 19.88 billion, and number of glial cells in gray matter ($N_g^{right\_gm}$) is 8.68 billion. Solving **eqs. S17** by assuming that the ratio of number of neurons to glial cells in the left and right hemispheres are equal, in the left hemisphere of the human brain we get $N_n^{left\_wm}$ = 1.42 billion, $N_n^{left\_gm}$ = 7.46 billion, $N_g^{left\_wm}$ = 21.81 billion, and $N_g^{left\_gm}$ = 10.47 billion. Thus the total number of neurons and glial cells number in gray and white matter are given by N_n^{gm} = 13.64 billion, N_n^{wm} = 2.71 billion, N_g^{gm} = 19.15 billion, and N_n^{wm} = 41.69 billion.

SI Text, Section E - Masses of gray and white matter of human cerebrum

The mass of the human cerebrum ($M_{cerebrum}$ = 1233 g) is separated in terms of white matter (M_{wm}) and gray matter (M_{gm})

$$M_{cerebrum} = M_{wm} + M_{gm}. \quad \text{(S18)}$$

Although M_{wm} and M_{gm} are unknown, each parameter has left and right hemispheric terms

$$M_{wm} = M_{wm}^{left} + M_{wm}^{right} \quad \text{(S19a)}$$

$$M_{gm} = M_{gm}^{left} + M_{gm}^{right} \quad \text{(S19b)}$$

where values of the right hemispheric terms have been reported as $M_{wm}^{right} = 294.22$ g and $M_{gm}^{right} = 316.26$ g[1]. By assuming that the mass ratio between white matter and gray matter (i.e., $r_{wg} = M_{wm}^{right} / M_{gm}^{right} = 0.9303$) is the same in the two hemispheres[1],

$$r_{wg} = M_{wm}^{right} / M_{gm}^{right} = M_{wm}^{left} / M_{gm}^{left} = 0.9303 \quad \text{(S20)}$$

and by using **eqs. S18** and **S19**, we get $M_{gm}^{left} = 322.11$ g and $M_{wm}^{left} = 299.67$ g, which together with the right hemispheric values gives $M_{gm} = 638.37$ g and $M_{wm} = 593.89$ g. Hence M_{gm} and M_{wm} together give the 1232.26 g of the human cerebrum without the cerebellum.

SI Text, Section F - Masses of individual neuron and glial cell in gray and white matter

To calculate the averaged mass of an individual neuron and glial cell in gray and white matter, for simplicity, and as a recent report suggests [25], we assumed that all types of glial cells have an equal mass value m_g, and all types of neurons have an equal mass value m_n, hence

$$M_{wm} = N_g^{wm} m_g + N_n^{wm} m_n \quad \text{(S21a)}$$

$$M_{gm} = N_g^{gm} m_g + N_n^{gm} m_n \quad \text{(S21b)}$$

and hence based on values of N_n^{gm}, N_n^{wm}, N_g^{gm}, and N_g^{wm} **(Section D)** as well as M_{gm} and M_{wm} **(Section E)** we calculated values of $m_n = 29.5$ ng, $m_g = 12.3$ ng, respectively.

SUPPLEMENTARY: Tables and Figures

Table S1. Neuronal firing rate (Hz) and glucose consumption (CMR_{glc}) measured across behavioral states in rat somatosensory cortex. Neuronal activity, represented by spike rate, was measured with microelectrodes. CMR_{glc} was measured by [^{14}C]-2-deoxyglucose (2DG) autoradiography. See refs. [42-51] for 2DG and electrophysiology details. Supplementary Materials in Hyder et al [52] describe the details of these studies.

Behavioral state [#]	**PR** (refs. 42, 43)	**US1** (refs. 44, 45)	**AR** (refs. 46-48)	**AS** (refs. 46-48)	**UR** (refs. 45, 49)	**US2** (refs. 45, 49)	**CR** (refs. 50, 51)	**CS** (refs. 50, 51)	**HR** (refs. 50, 51)	**HS** (refs. 50, 51)
Neuronal firing rate (*f* in units of Hz)	0.00	4.25	3.10	3.40	3.70[¶]	5.30	2.60[□]	4.10[□]	3.20[§]	3.40[¥]
CMR_{glc} (μ mol/g/min)	0.21	0.96	0.88	0.97	0.68	0.96	0.52	0.73	0.65	0.68

[#] PR = pentobarbital; US = urethane stimulation; AR = awake rest; AS = awake stimulation; UR = urethane rest; US2 = urethane stimulation; CR = α-chloralose rest; CS = α-chloralose stimulation; HR = halothane rest; HS = halothane stimulation.

[¶] average of urethane anesthetized states with spike rates of 4.6 and 2.8 Hz as measured by matrix electrodes.

[§] upon sensory stimulation under urethane anesthesia spike rate increased by 1.6 Hz as measured by matrix electrodes.

[□] based on spike rate histograms with 84-7% at 1.0 Hz and 13-6% at 11 Hz and fractions of population are 3 times greater than HR.

[□] based on spike rate histograms with 84-7% at 3.1 Hz and 13-6% at 11 Hz and fractions of population are 3 times greater than HR.

[$] based on spike rate histograms with 34-5% at 6.9 Hz and 65-6% at 11 Hz and fractions of population are 3 times less than CR.

[¥] based on spike rate histograms with 34-5% at 8.7 Hz and 65-6% at 11 Hz and fractions of population are 3 times less than CS.

Table S2. Neuronal activity (f_{BIS}) and glucose consumption (CMR_{glc}) measured across behavioral states in human visual cortex. Neuronal activity, represented by bispectral index (BIS) as measured by electroencephalography (EEG). CMR_{glc} (μmol/g/min) was measured by positron emission tomography (PET) using the [^{18}F]-fluorodeoxyglucose (FDG) as the tracer. See refs. [53-59] and [57, 60-67] for PET and EEG details, respectively. Supplementary Materials in Hyder et al [52] describe the details of these studies.

Behavioral State#	**Neuronal Activity** (f_{BIS}, EEG recordings in BIS scale (0~100)	**CMR_{glc}** (μmol/g/min)
AWK (refs. [53-55, 60])	100	0.33
SLP (refs. [54, 55, 60, 61])	79	0.26
HR (refs. [56, 62, 63])	58	0.19
PRO (refs. [53, 57, 64, 65])	39	0.16
VGA (refs. [58, 66])	35	0.15
VGP (refs. [59, 67])	8	0.09

VGP = persistent vegetative; VGA = acute vegetative; PRO = propofol; SEV = sevoflurane; HR = halothane rest; SLP = non-REM sleep; AWK = awake.

Table S3. ^{13}C-MRS results from rat somatosensory [68-84] and human visual [85-98] cortices of glutamate neurotransmitter cycling (V_{cycle}) and neuronal glucose oxidation ($CMR_{glc(ox),N}$). Units of μmol/g/min.

Reference	Condition (underline values indicate mean)	V_{cycle}	$CMR_{glc(ox),N}$
Sibson NR et al (1998) (ref.[68])	pentobarbital (120 mg/kg, +30 mg/kg/hr), rat	0.01	0.08
Sibson NR et al (1998) (ref.[68])	α-chloralose (80 mg/kg, +30 mg/kg/hr), rat	0.13	0.27
Sibson NR et al (1998) (ref.[68])	morphine sulfate (50 mg/kg, +25 mg/kg/hr), rat	0.40	0.51
Choi IY et al (2002) (ref.[69])	pentobarbital (80 mg/kg/hr)	0.04	0.18
Oz G et al (2004) (ref.[70])	awake (in vivo), rat	0.51	0.58
de Graaf RA et al (2004) (ref.[71])	halothane (1.5%), gray matter, rat	0.31	0.40
de Graaf RA et al (2004) (ref.[71])	halothane (1.5%), white matter, rat	0.02	0.10
de Graaf RA et al (2004) (ref.[71])	halothane (1.5%), subcortical, rat	0.18	0.21
Patel AB et al (2004) (ref.[72])	halothane (2-3)%, rat	0.22	0.26
Patel AB et al (2004) (ref.[72])	halothane (2-3)%, seizure, rat	0.52	0.57
Patel AB et al (2005) (ref.[73])	pentobarbital (120 mg/kg, +30 mg/kg/hr), rat	0.02	0.17
Patel AB et al (2005) (ref.[73])	halothane (1%)	0.58	0.61
Yang J, Shen J (2005) (ref.[74])	α-chloralose (80 mg/kg, +27 mg/kg/hr), rat	0.16	0.25
Chowdhury GM et al (2007) (ref.[75])	urethane (1.5 g/kg), rat	0.28	0.28
Serres S et al (2008) (ref.[76])	pentobarbital (60 mg/kg), in vitro, rat	0.12	0.18
Serres S et al (2008) (ref.[76])	morphine sulfate (15 mg/kg), in vitro, rat	0.40	0.41
van Eijsden P et al (2010) (ref.[77])	halothane (2-3%), rat	0.27	0.24
Wang J et al (2010) (ref.[78])	awake (ex vivo), rat	0.49	0.54
Jiang L et al (2011) (ref.[79])	halothane (1%), rat	0.32	0.30
Duarte JM et al (2011) (ref.[80])	α-chloralose (80 mg/kg, +28 mg/kg/hr), rat	0.11	0.23
Duarte JM, Gruetter R (2013) (ref.[77])	α-chloralose (80 mg/kg, +28 mg/kg/hr), rat	0.16	0.18
Herzog RI et al (2013) (ref.[82])	isoflurane (1%), rat	0.35	0.44
Chowdhury GM et al (2014) (ref.[83])	awake (ex vivo), rat	0.55	0.56
Chowdhury GM et al (2014) (ref.[83])	pentobarbital (80 mg/kg/hr, ex vivo), rat	0.00	0.12
Lin AL et al (2014) (ref.[84])	young healthy (α-chloralose), rat	0.23	0.25
Lin AL et al (2014) (ref.[84])	aging healthy (α-chloralose), rat	0.13	0.13
Lin AL et al (2014) (ref.[84])	aging calorie restricted (α-chloralose), rat	0.23	0.20
Mason GF et al (1995) (ref.[85])	awake, human	<u>0.25</u>	0.37
Gruetter R et al (1998) (ref.[86])	awake, human	0.32	0.37
Shen J et al (1999) (ref.[87])	awake, human	0.32	0.36
Pan JW et al (2000) (ref.[88])	awake, human	<u>0.25</u>	0.33
Chhina N et al (2001) (ref.[89])	awake, human	0.29	0.38
Chen W et al (2001) (ref.[99])	awake, human	<u>0.25</u>	0.42
Gruetter R et al (2001) (ref.[91])	awake, human	0.17	0.29
Bluml et al (2002) (ref.[92])	awake, human	<u>0.25</u>	0.35
Lebon V et al (2002) (ref.[93])	awake, human	0.28	<u>0.34</u>
Mason GF et al (2007) (ref.[94])	awake, human	<u>0.25</u>	0.36
Henry PG et al (2010) (ref.[95])	awake, human	<u>0.25</u>	0.40
Boumezbeur F et al (2010) (ref.[96])	awake, human	0.16	0.27
Jiang L et al (2013) (ref.[97])	awake, human, light drinkers	0.17	<u>0.34</u>
Jiang L et al (2013) (ref.[97])	awake, human, heavy drinkers	0.26	<u>0.34</u>
Abdallah CG et al (2014) (ref.[98])	awake, human, depression	0.18	0.24

Table S4. Experimental results of glucose oxidation in astrocytes ($CMR_{glc(ox),A}$) compared to total glucose oxidation ($CMR_{glc(ox),T}$) measured by ^{13}C-MRS in rat and human brain. All human and rat data were localized to the visual and somatosensory cortices, respectively. All units in μmol/g/min. Supplementary Materials in Hyder et al [52] describe the details of these studies.

Reference	Condition	¶ $CMR_{glc(ox),A}$	§ $CMR_{glc(ox),T}$
Oz G et al (2004) J Neurosci. (ref.[70])	rat, awake	0.18	0.76
Shen J et al (1999) Proc Natil Acad Sci USA. (ref.[87])	human, awake	0.05	0.41
Bluml et al (2002) NMR Biomed. (ref.[92])	human, awake	0.07	0.42
Lebon V et al (2002) J Neurosci. (ref.[93])	human, awake	0.07	0.43
Gruetter R et al (2001) Am J Physiol. (ref.[91])	human, awake	0.08	0.37

¶ For all rat studies the full pyruvate carboxylase flux was used as a maximum estimate of $CMR_{glc(ox),A}$; see ref. [13] for details.
§ For all rat and human studies $CMR_{glc(ox),T}$ was estimated by adding neuronal ($CMR_{glc(ox),N}$) and astrocytic ($CMR_{glc(ox),A}$) glucose oxidation terms.

Table S5. Experimental results of glucose oxidation in inhibitory neurons ($CMR_{glc(ox),IN}$) compared to total glucose oxidation in neurons ($CMR_{glc(ox),N}$) measured by ^{13}C-MRS in rat and human brain. All human and rat data were localized to the visual and somatosensory cortices, respectively. All units in μmol/g/min. Supplementary Materials in Hyder et al [52] describe the details of these studies.

Reference	Condition	$CMR_{glc(ox),IN}$	$CMR_{glc(ox),N}$
Patel AB et al (2005) PNAS (ref.[73])	rat, pentobarbital	0.03	0.14
Patel AB et al (2005) PNAS (ref.[73])	rat, halothane	0.11	0.50
Abdallah CG et al (2014) Am J Psychiat. (ref.[98])	human, awake	¶ 0.04	¶ 0.19

¶ $CMR_{glc(ox),IN}$ / $CMR_{glc(ox),N}$ was estimated from the ratio of V_{GAD} / V_{cycle} in normal human brain [98], where V_{GAD} is the GABA synthesis rate and proportional to inhibitory neurotransmitter cycling ($V_{cycle(IN)}$) and V_{cycle} is the total neurotransmitter cycling, based on the assumption from findings in the rat that $V_{cycle(IN)}$ / V_{cycle} is proportional to $CMR_{glc(ox),IN}$ / $CMR_{glc(ox),N}$ [73].

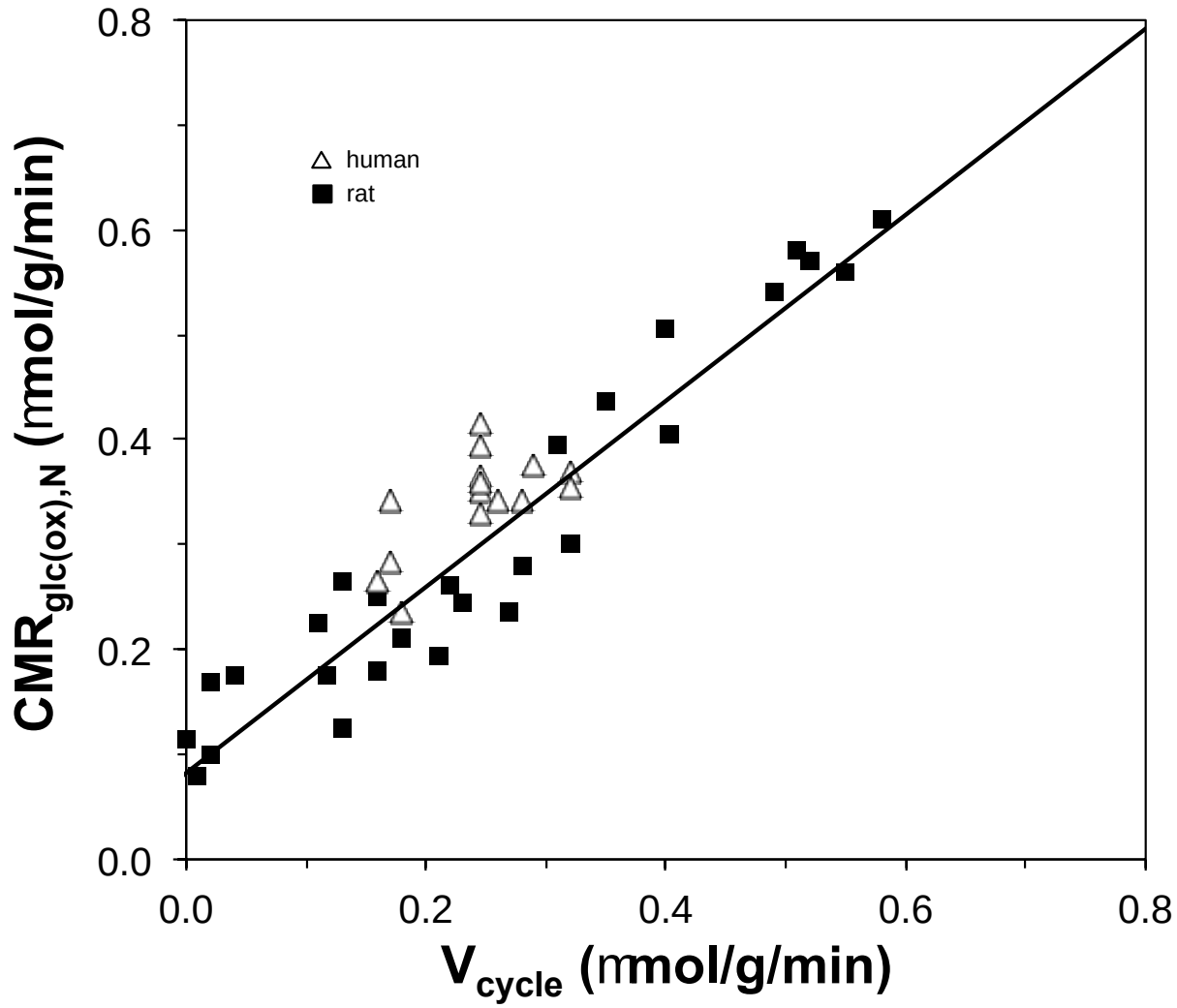

Figure S1. Relationship between neuronal activity (horizontal axis) and glucose metabolism (vertical axis) measured by ^{13}C-MRS in rat and human brain. Rates of total glutamate neurotransmitter cycling (V_{cycle}) and glucose oxidation in neurons ($CMR_{glc(ox),N}$) measured by ^{13}C-MRS. The 24 different data points in rat brain represent a variety of behavioral states in the somatosensory cortex (i.e., different levels of anesthesia, sleep, seizure, awake, etc.), whereas the 15 different data points in human brain represent different levels of partial volume in gray matter in the visual cortex. See **Table S3** for values of V_{cycle} and $CMR_{glc(ox),N}$. If the data for the rat and human brain have been normalized to the resting awake state values, these ^{13}C-MRS results suggest that in the resting awake state ~80% of neuronal energy consumption supports signaling events associated with neuronal activity, whereas ~20% of neuronal energy consumption supports nonsignaling functions because the line is the best-fit linear regression of the rat data (i.e., $CMR_{glc(ox),N} = 0.8\ V_{cycle} + 0.15$, $R^2 = 0.92$).

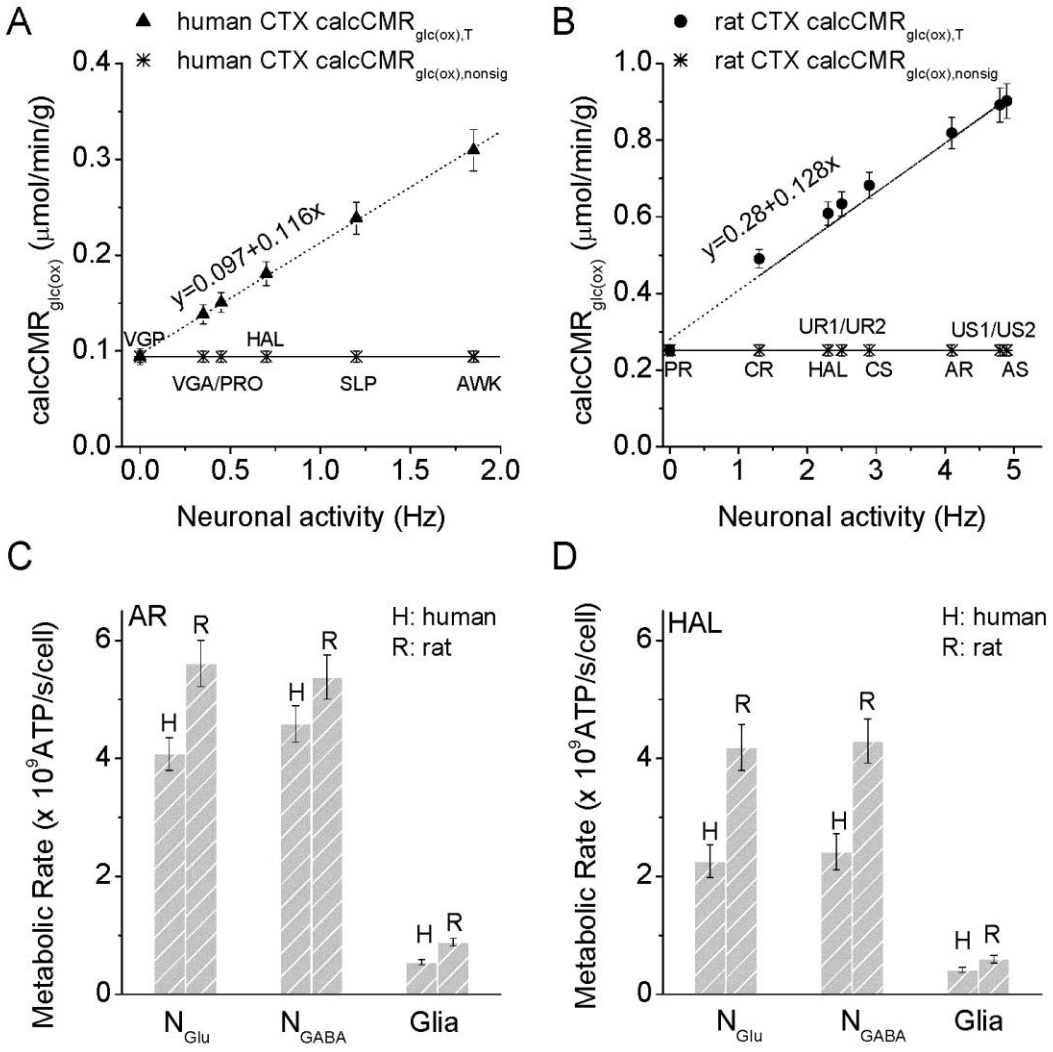

Figure S2. (A) For the human, values of $calcCMR_{glc(ox)}$ for signaling and nonsignaling components (i.e., $calcCMR_{glc(ox),T}$, triangles) and of only nonsignaling component, (i.e., $calcCMR_{glc(ox),nonsig}$, asterisk) across different behavioral states as a function of calcRate. See **Figure 1C** $calcCMR_{glc(ox),T}$ and calcRate values for human. The relationship between $calcCMR_{glc(ox),T}$ and calcRate is fitted by a linear function y=0.097+0.116x, with a correlation of R^2=0.98, while nonsignaling component of cortex $calcCMR_{glc(ox),nonsig}$ is invariant with calcRate. **(B)** For the rat, values of $calcCMR_{glc(ox)}$ for signaling and nonsignaling components (i.e., $calcCMR_{glc(ox),T}$, circles) and of only nonsignaling component (i.e., $calcCMR_{glc(ox),nonsig}$, asterisk) across different behavioral states as a function of calcRate. See **Figure 1B** $calcCMR_{glc(ox),T}$ and calcRate values for rat. The relationship between $calcCMR_{glc(ox),T}$ and calcRate is fitted by a linear function =0.28+0.128x, with a correlation of R^2=0.96, while nonsignaling components of cortex $calcCMR_{glc(ox),nonsig}$ is invariant with calcRate. **(C)** For cerebral cortex in awake resting state (AR in **Figure 1B** and **1C**) the basic metabolic rates for excitatory glutamatergic neurons (N_{Glu}), inhibitory GABAergic neurons (N_{GABA}), and glial cells (Glia) are 15-20% higher in rat (R) than in human (H), which is in part because human neurons have ~1 Hz mean firing rate that is lower than ~4 Hz in rat neurons in the awake state (see **Figures 1B** and **1C**). **(D)** For cerebral cortex in halothane anesthetized resting state (HR in **Figures 1B** and **1C**) the basic metabolic rates for N_{Glu} and N_{GABA} are reduced by nearly half in human (H) from the rat (R), but basic metabolic rates for Glia are about the same in human (H) and rat (R). All N_{Glu}, N_{GABA}, and Glia values in HR are decreased 20-40% because of firing rate drop from AR (see **Figures 1B** and **1C**).

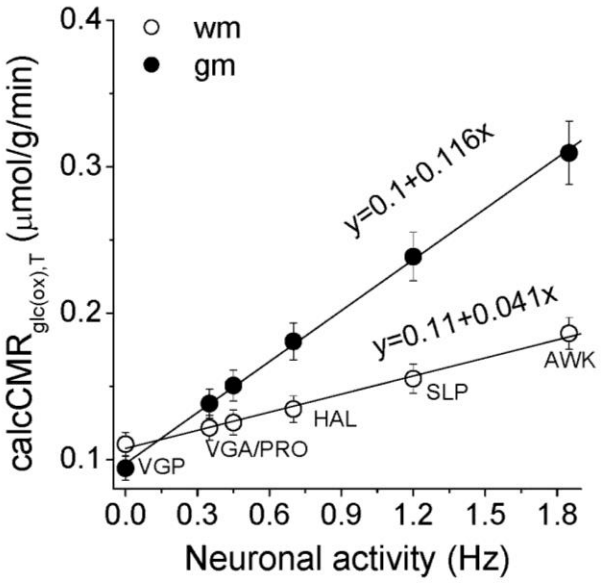

Figure S3. The calculated total $CMR_{glc(ox)}$ ($calcCMR_{glc(ox),T}$) for gray matter (GM, black circles) and white matter (WM, white circles) as a function of calculated neuronal activities (Neuronal Activity) for the different states shown in **Figures 1C** for the human.

REFERENCES

1. Azevedo FA, Carvalho LR, Grinberg LT, Farfel JM, Ferretti RE, Leite RE *et al.* Equal numbers of neuronal and nonneuronal cells make the human brain an isometrically scaled-up primate brain. *The Journal of comparative neurology* 2009; 513(5)**:** 532-41.

2. Kandel ER, Schwartz JH, Jessell TM. *Principles of neural science*, McGraw-Hill, Health Professions Division: New York, 2000.

3. McCormick DA, Connors BW, Lighthall JW, Prince DA. Comparative electrophysiology of pyramidal and sparsely spiny stellate neurons of the neocortex. *J Neurophysiol* 1985; 54(4)**:** 782-806.

4. Zonta M, Angulo MC, Gobbo S, Rosengarten B, Hossmann KA, Pozzan T *et al.* Neuron-to-astrocyte signaling is central to the dynamic control of brain microcirculation. *Nature neuroscience* 2003; 6(1)**:** 43-50.

5. Schummers J, Yu H, Sur M. Tuned responses of astrocytes and their influence on hemodynamic signals in the visual cortex. *Science* 2008; 320(5883)**:** 1638-43.

6. Matute C. Calcium dyshomeostasis in white matter pathology. *Cell Calcium* 2010; 47(2)**:** 150-7.

7. Metea MR, Newman EA. Glial cells dilate and constrict blood vessels: a mechanism of neurovascular coupling. *The Journal of neuroscience : the official journal of the Society for Neuroscience* 2006; 26(11)**:** 2862-70.

8. Belanger M, Allaman I, Magistretti PJ. Brain energy metabolism: focus on astrocyte-neuron metabolic cooperation. *Cell metabolism* 2011; 14(6)**:** 724-38.

9. Henry CJ. Basal metabolic rate studies in humans: measurement and development of new equations. *Public health nutrition* 2005; 8(7A)**:** 1133-52.

10. Baddeley H. *Physics and the Human Body: Stories of Who Discovered What*, AuthorHouse, 2008.

11. Kondepudi DK, Prigogine I. *Modern thermodynamics : from heat engines to dissipative structures*, John Wiley & Sons: Chichester; New York, 1998.

12. Gibson GE, Dienel GA, SpringerLink. Handbook of neurochemistry and molecular neurobiology. 2007.

13. Hyder F, Patel AB, Gjedde A, Rothman DL, Behar KL, Shulman RG. Neuronal-glial glucose oxidation and glutamatergic-GABAergic function. *Journal of cerebral blood flow and*

metabolism : official journal of the International Society of Cerebral Blood Flow and Metabolism 2006; 26(7)**:** 865-77.

14. Braitenberg V, Schüz A. *Cortex: statistics and geometry of neuronal connectivity*, Springer, 1998.

15. Shu YS, Duque A, Yu YG, Haider B, McCormick DA. Properties of action-potential initiation in neocortical pyramidal cells: Evidence from whole cell axon recordings. *Journal of Neurophysiology* 2007; 97(1)**:** 746-760.

16. Attwell D, Laughlin SB. An energy budget for signaling in the grey matter of the brain. *Journal of cerebral blood flow and metabolism : official journal of the International Society of Cerebral Blood Flow and Metabolism* 2001; 21(10)**:** 1133-45.

17. Howarth C, Gleeson P, Attwell D. Updated energy budgets for neural computation in the neocortex and cerebellum. *Journal of cerebral blood flow and metabolism : official journal of the International Society of Cerebral Blood Flow and Metabolism* 2012; 32(7)**:** 1222-32.

18. Jiang M, Zhu J, Liu YP, Yang MP, Tian CP, Jiang S *et al.* Enhancement of Asynchronous Release from Fast-Spiking Interneuron in Human and Rat Epileptic Neocortex. *PLoS biology* 2012; 10(5).

19. Mishima T, Hirase H. In Vivo Intracellular Recording Suggests That Gray Matter Astrocytes in Mature Cerebral Cortex and Hippocampus Are Electrophysiologically Homogeneous. *J. Neurosci.* 2010; 30(8)**:** 3093-3100.

20. Alle H, Roth A, Geiger JR. Energy-efficient action potentials in hippocampal mossy fibers. *Science* 2009; 325(5946)**:** 1405-8.

21. Carter BC, Bean BP. Sodium entry during action potentials of mammalian neurons: incomplete inactivation and reduced metabolic efficiency in fast-spiking neurons. *Neuron* 2009; 64(6)**:** 898-909.

22. Hasenstaub A, Otte S, Callaway E, Sejnowski TJ. Metabolic cost as a unifying principle governing neuronal biophysics. *Proceedings of the National Academy of Sciences of the United States of America* 2010; 107(27)**:** 12329-34.

23. Hallermann S, de Kock CP, Stuart GJ, Kole MH. State and location dependence of action potential metabolic cost in cortical pyramidal neurons. *Nature neuroscience* 2012; 15(7)**:** 1007-14.

24. Yu Y, Hill AP, McCormick DA. Warm Body Temperature Facilitates Energy Efficient Cortical Action Potentials. *PLoS computational biology* 2012; 8(4)**:** e1002456.

25. Mota B, Herculano-Houzel S. All brains are made of this: a fundamental building block of brain matter with matching neuronal and glial masses. *Frontiers in neuroanatomy* 2014; 8**:** 127.

26. Harris JJ, Attwell D. The energetics of CNS white matter. In: *The Journal of neuroscience : the official journal of the Society for Neuroscience*. 2012/01/06 ed, 2012. pp 356-71.

27. Hardingham NR, Larkman AU. Rapid report: the reliability of excitatory synaptic transmission in slices of rat visual cortex in vitro is temperature dependent. *The Journal of physiology* 1998; 507 (Pt 1)**:** 249-56.

28. Peyrache A, Dehghani N, Eskandar EN, Madsen JR, Anderson WS, Donoghue JA *et al.* Spatiotemporal dynamics of neocortical excitation and inhibition during human sleep. *Proceedings of the National Academy of Sciences of the United States of America* 2012; 109(5)**:** 1731-1736.

29. Kavanaugh M, Arriza JL, North R, Amara S. Electrogenic uptake of gamma-aminobutyric acid by a cloned transporter expressed in Xenopus oocytes. *Journal of Biological Chemistry* 1992; 267(31)**:** 22007-22009.

30. Lu C-C, Kabakov A, Markin VS, Mager S, Frazier GA, Hilgemann DW. Membrane transport mechanisms probed by capacitance measurements with megahertz voltage clamp. *Proceedings of the National Academy of Sciences* 1995; 92(24)**:** 11220-11224.

31. Loo DD, Eskandari S, Boorer KJ, Sarkar HK, Wright EM. Role of Cl− in electrogenic Na+-coupled cotransporters GAT1 and SGLT1. *Journal of Biological Chemistry* 2000; 275(48)**:** 37414-37422.

32. Lam K, Sefton AJ, Bennett MR. Loss of axons from the optic nerve of the rat during early postnatal development. *Brain research* 1982; 255(3)**:** 487-91.

33. Barres BA, Hart IK, Coles HS, Burne JF, Voyvodic JT, Richardson WD *et al.* Cell death and control of cell survival in the oligodendrocyte lineage. *Cell* 1992; 70(1)**:** 31-46.

34. Kettenmann H, Kirishchuk S, Verkhratskii A. Calcium signalling in oligodendrocytes. *Neurophysiology+* 1994; 26(1)**:** 21-25.

35. Fields RD. Oligodendrocytes changing the rules: action potentials in glia and oligodendrocytes controlling action potentials. *The Neuroscientist : a review journal bringing neurobiology, neurology and psychiatry* 2008; 14(6)**:** 540-3.

36. Kukley M, Capetillo-Zarate E, Dietrich D. Vesicular glutamate release from axons in white matter. *Nature neuroscience* 2007; 10(3)**:** 311-20.

37. Herculano-Houzel S, Mota B, Lent R. Cellular scaling rules for rodent brains. *Proceedings of the National Academy of Sciences of the United States of America* 2006; 103(32)**:** 12138-43.

38. Yu Y, Herman P, Rothman DL, Agarwal D, Hyder F. A validated human brain energy budget by ^{13}C MRS and 2DG autoradiography. In: *In submission*, 2016.

39. Jiang M, Zhu J, Liu Y, Yang M, Tian C, Jiang S *et al.* Enhancement of asynchronous release from fast-spiking interneuron in human and rat epileptic neocortex. *PLoS biology* 2012; 10(5)**:** e1001324.

40. Iber C, American Academy of Sleep M. *The AASM manual for the scoring of sleep and associated events : rules, terminology and technical specifications*, American Academy of Sleep Medicine: Westchester, Ill, 2007.

41. Csercsa R, Dombovari B, Fabo D, Wittner L, Eross L, Entz L *et al.* Laminar analysis of slow wave activity in humans. *Brain* 2010; 133(9)**:** 2814-29.

42. Sakabe T, Tsutsui T, Maekawa T, Ishikawa T, Takeshita H. Local cerebral glucose utilization during nitrous oxide and pentobarbital anesthesia in rats. *Anesthesiology* 1985; 63(3)**:** 262-6.

43. Crane PD, Braun LD, Cornford EM, Cremer JE, Glass JM, Oldendorf WH. Dose dependent reduction of glucose utilization by pentobarbital in rat brain. *Stroke; a journal of cerebral circulation* 1978; 9(1)**:** 12-8.

44. de Kock CP, Bruno RM, Spors H, Sakmann B. Layer- and cell-type-specific suprathreshold stimulus representation in rat primary somatosensory cortex. *The Journal of physiology* 2007; 581(Pt 1)**:** 139-54.

45. Cholet N, Pellerin L, Welker E, Lacombe P, Seylaz J, Magistretti P *et al.* Local injection of antisense oligonucleotides targeted to the glial glutamate transporter GLAST decreases the metabolic response to somatosensory activation. *Journal of cerebral blood flow and metabolism : official journal of the International Society of Cerebral Blood Flow and Metabolism* 2001; 21(4)**:** 404-12.

46. de Kock CP, Sakmann B. Spiking in primary somatosensory cortex during natural whisking in awake head-restrained rats is cell-type specific. *Proceedings of the National Academy of Sciences of the United States of America* 2009; 106(38)**:** 16446-50.

47. Crosby G, Crane AM, Sokoloff L. A comparison of local rates of glucose utilization in spinal cord and brain in conscious and nitrous oxide- or pentobarbital-treated rats. *Anesthesiology* 1984; 61(4)**:** 434-8.

48. Kossut M, Hand PJ, Greenberg J, Hand CL. Single vibrissal cortical column in SI cortex of rat and its alterations in neonatal and adult vibrissa-deafferented animals: a quantitative 2DG study. *J Neurophysiol* 1988; 60(2)**:** 829-52.

49. Erchova IA, Lebedev MA, Diamond ME. Somatosensory cortical neuronal population activity across states of anaesthesia. *Eur J Neurosci* 2002; 15(4)**:** 744-52.

50. Maandag NJ, Coman D, Sanganahalli BG, Herman P, Smith AJ, Blumenfeld H *et al.* Energetics of neuronal signaling and fMRI activity. *Proceedings of the National Academy of Sciences of the United States of America* 2007; 104(51)**:** 20546-51.

51. Ueki M, Mies G, Hossmann KA. Effect of alpha-chloralose, halothane, pentobarbital and nitrous oxide anesthesia on metabolic coupling in somatosensory cortex of rat. *Acta Anaesthesiol Scand* 1992; 36(4)**:** 318-22.

52. Hyder F, Rothman DL, Bennett MR. Cortical energy demands of signaling and nonsignaling components in brain are conserved across mammalian species and activity levels. *Proceedings of the National Academy of Sciences of the United States of America* 2013; 110(9)**:** 3549-54.

53. Alkire MT, Haier RJ, Barker SJ, Shah NK, Wu JC, Kao YJ. Cerebral metabolism during propofol anesthesia in humans studied with positron emission tomography. *Anesthesiology* 1995; 82(2)**:** 393-403; discussion 27A.

54. Heiss WD, Pawlik G, Herholz K, Wagner R, Wienhard K. Regional cerebral glucose metabolism in man during wakefulness, sleep, and dreaming. *Brain research* 1985; 327(1-2)**:** 362-6.

55. Buchsbaum MS, Gillin JC, Wu J, Hazlett E, Sicotte N, Dupont RM *et al.* Regional cerebral glucose metabolic rate in human sleep assessed by positron emission tomography. *Life sciences* 1989; 45(15)**:** 1349-56.

56. Alkire MT, Pomfrett CJ, Haier RJ, Gianzero MV, Chan CM, Jacobsen BP *et al.* Functional brain imaging during anesthesia in humans: effects of halothane on global and regional cerebral glucose metabolism. *Anesthesiology* 1999; 90(3)**:** 701-9.

57. Kaisti KK, Langsjo JW, Aalto S, Oikonen V, Sipila H, Teras M *et al.* Effects of sevoflurane, propofol, and adjunct nitrous oxide on regional cerebral blood flow, oxygen consumption, and blood volume in humans. *Anesthesiology* 2003; 99(3)**:** 603-13.

58. Laureys S. Functional neuroimaging in the vegetative state. *NeuroRehabilitation* 2004; 19(4)**:** 335-41.

59. Tommasino C, Grana C, Lucignani G, Torri G, Fazio F. Regional cerebral metabolism of glucose in comatose and vegetative state patients. *Journal of neurosurgical anesthesiology* 1995; 7(2)**:** 109-16.

60. Ozgoren M, Bayazit O, Kocaaslan S, Gokmen N, Oniz A. Brain function assessment in different conscious states. *Nonlinear biomedical physics* 2010; 4 Suppl 1**:** S6.

61. Tung A, Lynch JP, Roizen MF. Use of the BIS monitor to detect onset of naturally occurring sleep. *Journal of clinical monitoring and computing* 2002; 17(1)**:** 37-42.

62. Umamaheswara Rao GS, Ali Z, Ramamoorthy M, Patil J. Equi-MAC concentrations of halothane and isoflurane do not produce similar bispectral index values. *Journal of neurosurgical anesthesiology* 2007; 19(2)**:** 93-6.

63. Schwab HS, Seeberger MD, Eger EI, 2nd, Kindler CH, Filipovic M. Sevoflurane decreases bispectral index values more than does halothane at equal MAC multiples. *Anesthesia and analgesia* 2004; 99(6)**:** 1723-7, table of contents.

64. Leslie K, Sleigh J, Paech MJ, Voss L, Lim CW, Sleigh C. Dreaming and electroencephalographic changes during anesthesia maintained with propofol or desflurane. *Anesthesiology* 2009; 111(3)**:** 547-55.

65. Bjornsson MA, Norberg A, Kalman S, Karlsson MO, Simonsson US. A two-compartment effect site model describes the bispectral index after different rates of propofol infusion. *Journal of pharmacokinetics and pharmacodynamics* 2010; 37(3)**:** 243-55.

66. Pandit JJ, Schmelzle-Lubiecki B, Goodwin M, Saeed N. Bispectral index-guided management of anaesthesia in permanent vegetative state. *Anaesthesia* 2002; 57(12)**:** 1190-4.

67. Dunham CM, Katradis DA, Williams MD. The bispectral index, a useful adjunct for the timely diagnosis of brain death in the comatose trauma patient. *American journal of surgery* 2009; 198(6)**:** 846-51.

68. Sibson NR, Dhankhar A, Mason GF, Rothman DL, Behar KL, Shulman RG. Stoichiometric coupling of brain glucose metabolism and glutamatergic neuronal activity. *Proceedings of the National Academy of Sciences of the United States of America* 1998; 95(1)**:** 316-21.

69. Choi IY, Lei H, Gruetter R. Effect of deep pentobarbital anesthesia on neurotransmitter metabolism in vivo: on the correlation of total glucose consumption with glutamatergic action. *Journal of cerebral blood flow and metabolism : official journal of the International Society of Cerebral Blood Flow and Metabolism* 2002; 22(11)**:** 1343-51.

70. Oz G, Berkich DA, Henry PG, Xu Y, LaNoue K, Hutson SM *et al.* Neuroglial metabolism in the awake rat brain: CO2 fixation increases with brain activity. *J Neurosci* 2004; 24(50)**:** 11273-9.

71. de Graaf RA, Mason GF, Patel AB, Rothman DL, Behar KL. Regional glucose metabolism and glutamatergic neurotransmission in rat brain in vivo. *Proceedings of the National Academy of Sciences of the United States of America* 2004; 101(34)**:** 12700-5.

72. Patel AB, de Graaf RA, Mason GF, Kanamatsu T, Rothman DL, Shulman RG *et al.* Glutamatergic neurotransmission and neuronal glucose oxidation are coupled during intense neuronal activation. *Journal of cerebral blood flow and metabolism : official journal of the International Society of Cerebral Blood Flow and Metabolism* 2004; 24(9)**:** 972-85.

73. Patel AB, de Graaf RA, Mason GF, Rothman DL, Shulman RG, Behar KL. The contribution of GABA to glutamate/glutamine cycling and energy metabolism in the rat cortex in vivo. *Proceedings of the National Academy of Sciences of the United States of America* 2005; 102(15)**:** 5588-93.

74. Yang J, Shen J. In vivo evidence for reduced cortical glutamate-glutamine cycling in rats treated with the antidepressant/antipanic drug phenelzine. *Neuroscience* 2005; 135(3)**:** 927-37.

75. Chowdhury GM, Patel AB, Mason GF, Rothman DL, Behar KL. Glutamatergic and GABAergic neurotransmitter cycling and energy metabolism in rat cerebral cortex during postnatal development. *Journal of cerebral blood flow and metabolism : official journal of the International Society of Cerebral Blood Flow and Metabolism* 2007; 27(12)**:** 1895-907.

76. Serres S, Raffard G, Franconi JM, Merle M. Close coupling between astrocytic and neuronal metabolisms to fulfill anaplerotic and energy needs in the rat brain. *Journal of cerebral blood flow and metabolism : official journal of the International Society of Cerebral Blood Flow and Metabolism* 2008; 28(4)**:** 712-24.

77. van Eijsden P, Behar KL, Mason GF, Braun KP, de Graaf RA. In vivo neurochemical profiling of rat brain by 1H-[13C] NMR spectroscopy: cerebral energetics and glutamatergic/GABAergic neurotransmission. *Journal of neurochemistry* 2010; 112(1)**:** 24-33.

78. Wang J, Jiang L, Jiang Y, Ma X, Chowdhury GM, Mason GF. Regional metabolite levels and turnover in the awake rat brain under the influence of nicotine. *Journal of neurochemistry* 2010; 113(6)**:** 1447-58.

79. Jiang L, Mason GF, Rothman DL, de Graaf RA, Behar KL. Cortical substrate oxidation during hyperketonemia in the fasted anesthetized rat in vivo. *Journal of cerebral blood flow and metabolism : official journal of the International Society of Cerebral Blood Flow and Metabolism* 2011; 31(12)**:** 2313-23.

80. Duarte JM, Lanz B, Gruetter R. Compartmentalized Cerebral Metabolism of [1,6-C]Glucose Determined by in vivoC NMR Spectroscopy at 14.1 T. *Frontiers in neuroenergetics* 2011; 3**:** 3.

81. Duarte JM, Gruetter R. Glutamatergic and GABAergic energy metabolism measured in the rat brain by (13) C NMR spectroscopy at 14.1 T. *Journal of neurochemistry* 2013; 126(5)**:** 579-90.

82. Herzog RI, Jiang L, Herman P, Zhao C, Sanganahalli BG, Mason GF *et al.* Lactate preserves neuronal metabolism and function following antecedent recurrent hypoglycemia. *The Journal of clinical investigation* 2013; 123(5)**:** 1988-98.

83. Chowdhury GM, Jiang L, Rothman DL, Behar KL. Ketone bodies support mainly basal over activity dependent neuronal oxidation in vivo. *Journal of cerebral blood flow and metabolism : official journal of the International Society of Cerebral Blood Flow and Metabolism* 2014; 34**:** 1233-1242.

84. Lin AL, Coman D, Jiang L, Rothman DL, Hyder F. Caloric restriction impedes age-related decline of mitochondrial function and neuronal activity. *Journal of cerebral blood flow and metabolism : official journal of the International Society of Cerebral Blood Flow and Metabolism* 2014; 34(9)**:** 1440-3.

85. Mason GF, Gruetter R, Rothman DL, Behar KL, Shulman RG, Novotny EJ. Simultaneous determination of the rates of the TCA cycle, glucose utilization, alpha-ketoglutarate/glutamate exchange, and glutamine synthesis in human brain by NMR. *Journal of cerebral blood flow and metabolism : official journal of the International Society of Cerebral Blood Flow and Metabolism* 1995; 15(1)**:** 12-25.

86. Gruetter R, Seaquist ER, Kim S, Ugurbil K. Localized in vivo ^{13}C-NMR of glutamate metabolism in the human brain: initial results at 4 tesla. *Dev Neurosci* 1998; 20(4-5)**:** 380-8.

87. Shen J, Petersen KF, Behar KL, Brown P, Nixon TW, Mason GF *et al.* Determination of the rate of the glutamate/glutamine cycle in the human brain by in vivo 13C NMR. *Proceedings of the National Academy of Sciences of the United States of America* 1999; 96(14)**:** 8235-40.

88. Pan JW, Stein DT, Telang F, Lee JH, Shen J, Brown P *et al.* Spectroscopic imaging of glutamate C4 turnover in human brain. *Magn Reson Med* 2000; 44(5)**:** 673-9.

89. Chhina N, Kuestermann E, Halliday J, Simpson LJ, Macdonald IA, Bachelard HS *et al.* Measurement of human tricarboxylic acid cycle rates during visual activation by (13)C magnetic resonance spectroscopy. *Journal of neuroscience research* 2001; 66(5)**:** 737-46.

90. Chen W, Zhu XH, Gruetter R, Seaquist ER, Adriany G, Ugurbil K. Study of tricarboxylic acid cycle flux changes in human visual cortex during hemifield visual stimulation using (1)H-[(13)C] MRS and fMRI. *Magn Reson Med* 2001; 45(3)**:** 349-55.

91. Gruetter R, Seaquist ER, Ugurbil K. A mathematical model of compartmentalized neurotransmitter metabolism in the human brain. *American journal of physiology. Endocrinology and metabolism* 2001; 281(1)**:** E100-12.

92. Bluml S, Moreno-Torres A, Shic F, Nguy CH, Ross BD. Tricarboxylic acid cycle of glia in the in vivo human brain. *NMR in biomedicine* 2002; 15(1)**:** 1-5.

93. Lebon V, Petersen KF, Cline GW, Shen J, Mason GF, Dufour S *et al.* Astroglial contribution to brain energy metabolism in humans revealed by 13C nuclear magnetic resonance spectroscopy: elucidation of the dominant pathway for neurotransmitter glutamate repletion and measurement of astrocytic oxidative metabolism. *J Neurosci* 2002; 22(5)**:** 1523-31.

94. Mason GF, Petersen KF, de Graaf RA, Shulman GI, Rothman DL. Measurements of the anaplerotic rate in the human cerebral cortex using 13C magnetic resonance spectroscopy and [1-13C] and [2-13C] glucose. *Journal of neurochemistry* 2007; 100(1)**:** 73-86.

95. Henry PG, Criego AB, Kumar A, Seaquist ER. Measurement of cerebral oxidative glucose consumption in patients with type 1 diabetes mellitus and hypoglycemia unawareness using (13)C nuclear magnetic resonance spectroscopy. *Metabolism* 2010; 59(1)**:** 100-6.

96. Boumezbeur F, Mason GF, de Graaf RA, Behar KL, Cline GW, Shulman GI *et al.* Altered brain mitochondrial metabolism in healthy aging as assessed by in vivo magnetic resonance spectroscopy. *Journal of cerebral blood flow and metabolism : official journal of the International Society of Cerebral Blood Flow and Metabolism* 2010; 30(1)**:** 211-21.

97. Jiang L, Gulanski BI, De Feyter HM, Weinzimer SA, Pittman B, Guidone E *et al.* Increased brain uptake and oxidation of acetate in heavy drinkers. *The Journal of clinical investigation* 2013; 123(4)**:** 1605-14.

98. Abdallah CG, Jiang L, De Feyter HM, Fasula M, Krystal JH, Rothman DL *et al.* Glutamate metabolism in major depressive disorder. *Am J Psychiatry* 2014; 171**:** 1320-1327.

99. Chen AC. New perspectives in EEG/MEG brain mapping and PET/fMRI neuroimaging of human pain. *Int J Psychophysiol* 2001; 42(2)**:** 147-59.